Acta Crystallographica Section D
Biological Crystallography
ISSN 1399-0047

The structural basis of the Tle4–Tli4 complex reveals the self-protection mechanism of H2-T6SS in *Pseudomonas aeruginosa*

Defen Lu,[a,b] Youshi Zheng,[a,b] Naishun Liao,[a,b] Ling Wei,[c] Bo Xu,[a,b] Xiaolong Liu[a,b]* and Jingfeng Liu[a,b,d]*

[a]The United Innovation of Mengchao Hepatobiliary Technology Key Laboratory of Fujian Province, MengChao Hepatobiliary Hospital of Fujian Medical University, Fuzhou 350025, People's Republic of China, [b]The Liver Center of Fujian Province, Fujian Medical University, Fuzhou 350025, People's Republic of China, [c]Beijing Center for Physical and Chemical Analysis, Beijing 100094, People's Republic of China, and [d]Liver Disease Center, The First Affiliated Hospital of Fujian Medical University, Fuzhou 350005, People's Republic of China

Correspondence e-mail: xiaoloong.liu@gmail.com, drjingfeng@126.com

Received 7 August 2014
Accepted 30 October 2014

PDB reference: Tle4–Tli4 complex, 4r1d

The type VI secretion system (T6SS) has recently been demonstrated to mediate interbacterial competition and to discriminate between self and nonself. T6SS$^+$ bacteria employ toxic effectors to inhibit rival cells and concurrently use effector cognate immunity proteins to protect their sibling cells. The effector and immunity pairs (E–I pairs) endow the bacteria with a great advantage in niche competition. Tle4–Tli4 (PA1510–PA1509) is a newly identified E–I pair that is controlled by H2-T6SS in *Pseudomonas aeruginosa*. Tle4 exhibits phospholipase activity, which destroys the cell membrane of rival cells, and the periplasm-located Tli4 in donor cells eliminates this toxic effect of Tle4. In this paper, the structure of the Tle4–Tli4 complex is reported at 1.75 Å resolution. Tle4 consists of two domains: a conserved α/β-hydrolase domain and an unusual cap domain in which two lid regions (lid1 and lid2) display a closed conformation that buries the catalytic triad in a deep funnel. Tli4 also displays a two-domain structure, in which a large lobe and a small lobe form a crab claw-like conformation. Tli4 uses this crab claw to grasp the cap domain of Tle4, especially the lid2 region, which prevents the interfacial activation of Tle4 and thus causes enzymatic dysfunction of Tle4 in sister cells.

1. Introduction

The bacterial type VI secretion system (T6SS) is a versatile and dynamic macromolecular machine that mediates the interactions of bacteria with both prokaryotic rivals and eukaryotic hosts (Filloux, 2013; Coulthurst, 2013; Ho *et al.*, 2014; Kapitein & Mogk, 2013). The T6SS is present in at least one-third of sequenced Gram-negative bacteria, especially in the Proteobacteria phylum (Bingle *et al.*, 2008). The secretion system comprises 13 core components (type 6 subunits/Tss) that form a macromolecular complex spanning the cell envelope and puncturing the recipient cell (Cascales & Cambillau, 2012; Silverman *et al.*, 2012). The T6SS is believed to be structurally and functionally homologous to the tail of bacteriophages (Leiman *et al.*, 2009; Pell *et al.*, 2009; Brunet *et al.*, 2014), and the contraction of this device injects the substrates or effector proteins into the recipient cells in a single shot (Ho *et al.*, 2014). These effector proteins play an important role in contributing to the ecology of the bacterial community and to the outcome of bacterial pathogenesis (Russell *et al.*, 2014).

Recently, considerable progress has been made in identification of the effectors of the T6SS (Benz & Meinhart, 2014; Russell *et al.*, 2014; Durand *et al.*, 2014). These effectors display a wide range of prokaryotic or eukaryotic cell toxicity. Valine–glycine repeat (VgrG) proteins fused with other domains in their C-terminus can act as the toxins of the T6SS.

For example, the actin cross-linking domain (ACD) in VgrG1 and the peptidoglycan hydrolase domain in VgrG3 from *Vibrio cholerae* target eukaryotic and prokaryotic cells, respectively (Pukatzki *et al.*, 2007; Brooks *et al.*, 2013; Dong, Ho *et al.*, 2013), the VgrG1 protein from *Aeromonas hydrophila* functions as a toxin by ADP ribosylation of actin (Suarez *et al.*, 2010) and VgrG5 expressed by *Burkholderia pseudomallei* and *B. thailandensis* promotes cell membrane fusion and thereby facilitates the spreading of these pathogens (Schwarz *et al.*, 2014; Toesca *et al.*, 2014). In addition to these VgrG-borne effectors, diverse VgrG-independent effectors that target distinct cell structures have been identified. For example, members of the type VI secretion amidase effector (Tae) and type VI secretion glycoside hydrolase effector (Tge) superfamilies destroy the distinctive bonds of murein in bacteria (Russell *et al.*, 2011, 2012; Whitney *et al.*, 2013), the type VI lipase effector (Tle) superfamily proteins and pore-forming toxins (*V. cholerae* VasX, *B. thailandensis* BTH_I2691 and *P. aeruginosa* PA14_69520 proteins) can cause membrane permeabilization (Dong, Ho *et al.*, 2013; Russell *et al.*, 2013; Jiang *et al.*, 2014; Miyata *et al.*, 2013; Hachani *et al.*, 2014) and rearrangement hotspot A and B (RhsA and RhsB) proteins from *Dickeya dadantii* and the type VI DNase effector (Tde) nuclease family in *Agrobacterium tumefaciens* target the genetic material (Koskiniemi *et al.*, 2013; Ma *et al.*, 2014). Moreover, Tse2, Tse4, Tse5 and Tse6, which are controlled by H1-T6SS in *Pseudomonas aeruginosa* (PAO1), are toxic to the recipient cells by an unknown mechanism (Hood *et al.*, 2010; Whitney *et al.*, 2014). Collectively, the T6SS effectors exhibit versatile and diverse properties.

The members of the Tle superfamily are newly discovered effectors that are controlled by H2-T6SS (Russell *et al.*, 2013). The Tle cognate immunity proteins (Tlis) can directly disable the transported Tle protein and thereby mediate the self-protection process. The Tle–Tli effector–immunity (E–I) pairs confer substantial advantage to the donor cell during inter-bacterial competition. The Tle superfamily can be divided into five groups (Tle1–Tle5) based on their distinct phospholipase activities, which selectively degrade the ester bonds (Russell *et al.*, 2013). Tle1–Tle4 contain a conserved G-*X*-S-*X*-G (where *X* denotes any residue) motif and exhibit phospholipase A_1 or A_2 (PLA_1 or PLA_2) activity, whereas Tle5 features a conserved H-*X*-K-*X*-*X*-*X*-*X*-D motif and exhibits phospholipase D (PLD) activity. Except for possessing the conserved catalytic motif, Tle1–Tle5 show no sequence similarities to known lipases, indicating that these proteins might use distinctive substrate-recognition and regulation mechanisms. In another aspect, because the effectors of T6SS are involved in the pathogenesis of the bacterium, they have potential as targets for antibacterial interference. Therefore, it is necessary to solve the structure of the Tle and Tli proteins. In this study, we selected Tle4 (PA1510) and Tli4 (PA1509) from *Pseudomonas aeruginosa* as our research model; by searching the Protein Data Bank (PDB) using their sequences, it was shown that these proteins contain no recognized folds, thus revealing their unique structural characteristics. We determined the Tle4–Tli4 complex structure, and this structure shows that Tle4 is an unusual lipase and that Tli4 inhibits Tle4 in a manner which is different from the mode observed in hitherto solved structures of E–I pairs.

2. Experimental procedures

2.1. Cloning, expression and purification of the Tle4–Tli4 complex

The genes encoding full-length Tle4 and an N-terminal 33-amino-acid truncation of Tli4 were PCR-amplified from *P. aeruginosa* PAO1 genomic DNA using oligonucleotide primers with *Nde*I and *Xho*I restriction recognition sites at the 5′ end and the 3′ end, respectively. The gene of Tle4 was constructed into pET-15b (Novagen, Germany), resulting in an N-terminally His_6-tagged protein. The Tli4 coding sequence was inserted into pET-30a expression vector with a stop codon at the 3′ end, resulting in nontagged protein. These two expression vectors were co-transformed into *Escherichia coli* BL21 (DE3) cells.

E. coli BL21 (DE3) cells harbouring the plasmids for Tle4 and Tli4 were grown in Luria Broth (LB) medium supplemented with 100 µg ml^{-1} ampicillin and 50 µg ml^{-1} kanamycin. When the OD_{600} reached 0.6, the incubation temperature was adjusted to 15°C and isopropyl β-D-1-thiogalactopyranoside (IPTG) was added to a final concentration of 0.1 m*M* to induce the expression of Tle4 and Tli4. About 12 h later, the cells were collected by centrifugation. The pellets were resuspended in buffer *A* (20 m*M* Tris–HCl pH 8.0, 200 m*M* NaCl) and lysed by sonication. The supernatant containing the recombinant Tle4–Tli4 complex was obtained by centrifugation at 28 500*g* for 45 min and was then applied onto an Ni-chelating Sepharose (GE Healthcare) affinity column pre-equilibrated with buffer *A*. The affinity column was washed with buffer *B* (20 m*M* Tris–HCl buffer pH 8.0, 100 m*M* NaCl, 5 m*M* imidazole). The Tle4–Tli4 complex was eluted with buffer *C* (20 m*M* Tris–HCl buffer pH 8.0, 100 m*M* NaCl, 250 m*M* imidazole). The eluate was further purified using a Superdex 200 size-exclusion column (GE Healthcare) in 10 m*M* Tris–HCl pH 8.0, 100 m*M* NaCl. The fractions containing the purified Tle4–Tli4 complex were collected according to protein purity as analyzed by SDS–PAGE and the final protein concentration used for crystallization was 15 mg ml^{-1}. Selenomethionine (SeMet)-labelled Tle4–Tli4 complex was also expressed in *E. coli* BL21 (DE3) cells, which were grown in SeMet-containing medium using the metabolic inhibition pathway (Van Duyne *et al.*, 1993), and was purified using the same procedure as used for the native Tle4–Tli4 complex. The SeMet-Tle4–Tli4 complex was concentrated to 15 mg ml^{-1} in buffer consisting of 10 m*M* Tris–HCl pH 8.0, 100 m*M* NaCl for crystallization. All protein purifications were performed at 4°C.

2.2. Crystallization and data collection

The crystals of Tle4–Tli4 and SeMet-labelled Tle4–Tli4 were grown by the hanging-drop vapour-diffusion method at 18°C using equal volumes of protein solution and reservoir

solution. All crystals were grown in the same reservoir solution consisting of 20%(*w*/*v*) PEG 3350, 0.1 *M* bis-tris pH 6.5. To prevent radiation damage, all crystals were cryoprotected with reservoir buffer containing 25% glycerol. All data sets were collected on beamline 17U1 at the Shanghai Synchrotron Radiation Facility using a charge-coupled device (CCD) detector and were processed using *HKL*-2000 (Otwinowski & Minor, 1997).

2.3. Structure determination and refinement

The structure of Tle4–Tli4 was determined by single-wavelength anomalous dispersion (SAD) phasing using the *PHENIX* software package (Adams *et al.*, 2002). The heavy atoms were found by *SOLVE* (Terwilliger & Berendzen, 1999). The initial phases were further improved and a SeMet-derivative model was built by *RESOLVE* (Terwilliger, 2000). The model was extended to higher resolution using the native data set and was refined with *PHENIX*. *Coot* (Emsley & Cowtan, 2004) and *LSQKAB* (Kabsch, 1976) were used for structure analysis. Data-collection and structure-refinement statistics for the SeMet and native Tle4–Tli4 complexes are given in Table 1. All molecular-graphic figures were rendered using *PyMOL* (http://www.pymol.org).

2.4. Dynamic light scattering (DLS)

DLS was used to detect the oligomeric state of the Tle4–Tli4 complex. The experiments were performed using a DynaPro dynamic light-scattering instrument (Protein Solutions). The proteins were diluted to 0.1 mg ml^{-1} in 10 m*M* Tris–HCl pH 8.0, 100 m*M* NaCl. Data were acquired at 25°C. Regularization histogram analyses of the DLS results were carried out using *DYNAMICS* v.5.25.44.

2.5. Gel-filtration assay

The Tle4–Tli4 complex was subjected to gel-filtration analysis (Superdex 200 10/300 GL column; GE Healthcare) in buffer consisting of 10 m*M* Tris–HCl pH 8.0, 100 m*M* NaCl. The assay was performed at a flow rate of 0.5 ml min^{-1} and an injection volume of 0.5 ml buffer containing Tle4–Tli4 complex (about 2 mg ml^{-1}) at 25°C. The elution volume of the Tle4–Tli4 complex was 13.9 ml under the conditions of the assay, corresponding to the molecular weight of their monomeric state. The protein was visualized by SDS–PAGE followed by Coomassie Blue staining.

3. Results

3.1. Overall structure of the Tle4–Tli4 complex

The structure of the Tle4–Tli4 complex was determined by SAD phasing using SeMet-derivative protein and was further refined to 1.75 Å resolution using the native data. The native crystal belonged to space group $P2_1$; there is one heterodimer complex molecule per asymmetric unit (Fig. 1*a*) and the molar ratio of Tle4 and Tli4 is in line with the 1:1 stoichiometry observed in solution (Figs. 1*b* and 1*c*). The complex structure displays a T-shaped form, with Tle4 located horizontally and being half-trapped by Tli4 at the bottom (Fig. 1*a*). Residues 1–44 and 562–569 of Tle4 and 334–380 of Tli4 lack interpretable electron densities, and thus our final model includes the core structures of Tle4 (residues 44–561) and Tli4 (residues 34–333) (Fig. 2*a*).

Table 1
Data-collection and refinement statistics.

Each data set was collected from a single crystal. Values in parentheses are for the highest resolution shell.

	Native Tle4–Tli4 complex	SeMet-derivative Tle4–Tli4 complex
Data collection		
Space group	$P2_1$	$P2_12_12_1$
Unit-cell parameters (Å, °)	a = 59.68, b = 135.18, c = 62.61, $\alpha = \gamma$ = 90.0, β = 113.5	a = 76.73, b = 111.05, c = 134.32, $\alpha = \beta = \gamma$ = 90.0
Wavelength (Å)	0.9790	0.9790 [peak]
Resolution (Å)	50–1.75 (1.81–1.75)	50–2.15 (2.23–2.15)
R_{merge} (%)	6.9 (44.5)	9.2 (45.1)
$\langle I/\sigma(I)\rangle$	25.5 (2.8)	52.46 (9.3)
Completeness (%)	94.4 (89.3)	99.8 (99.3)
Multiplicity	3.6 (3.7)	13.7 (13.6)
Refinement		
Resolution (Å)	20.00–1.74	
No. of reflections	86321	
R_{work}/R_{free} (%)	17.51/21.42	
No. of atoms		
Protein	6530	
Ca	1	
Water	960	
B factors (Å^2)		
Protein	23.2	
Ligand/ion	22.2	
Water	32.4	
R.m.s. deviations		
Bond lengths (Å)	0.007	
Bond angles (°)	1.065	
Ramachandran plot† (%)		
Most favoured	95.76	
Allowed	3.87	
Outliers	0.37	

† As defined in *PROCHECK*.

3.2. Structure of Tle4 in a closed conformation

Tle4 in the complex contains 18 α-helices, 15 β-strands and eight 3_{10}-helices and adopts a tandem two-domain structure with a canonical lipase-fold (a subset of the α/β-hydrolase fold) domain at one end and an unusual cap domain at the other end (Fig. 2*b* and Supplementary Fig. S1[1]). The lipase-fold domain consists of six parallel β-strands (β1, β7, β8, β9, β12 and β15) flanked by ten α-helices (with α3, α4, α5 and α18 located on one side and α6, α7, α8, α9, α16 and α17 located on the other side). Although the topology of this type of fold is highly conserved in the α/β-hydrolase superfamily, variations are still observed in Tle4 (Figs. 2*c* and 2*d*). Typically eight central β-strands are present, but the first two strands are absent in Tle4. The number of surrounding α-helices in Tle4 is also distinct, and one short β-sheet is inserted between α4 and α5. Moreover, a metal ion-binding motif connecting α4 and β7

[1] Supporting information has been deposited in the IUCr electronic archive (Reference: DW5114).

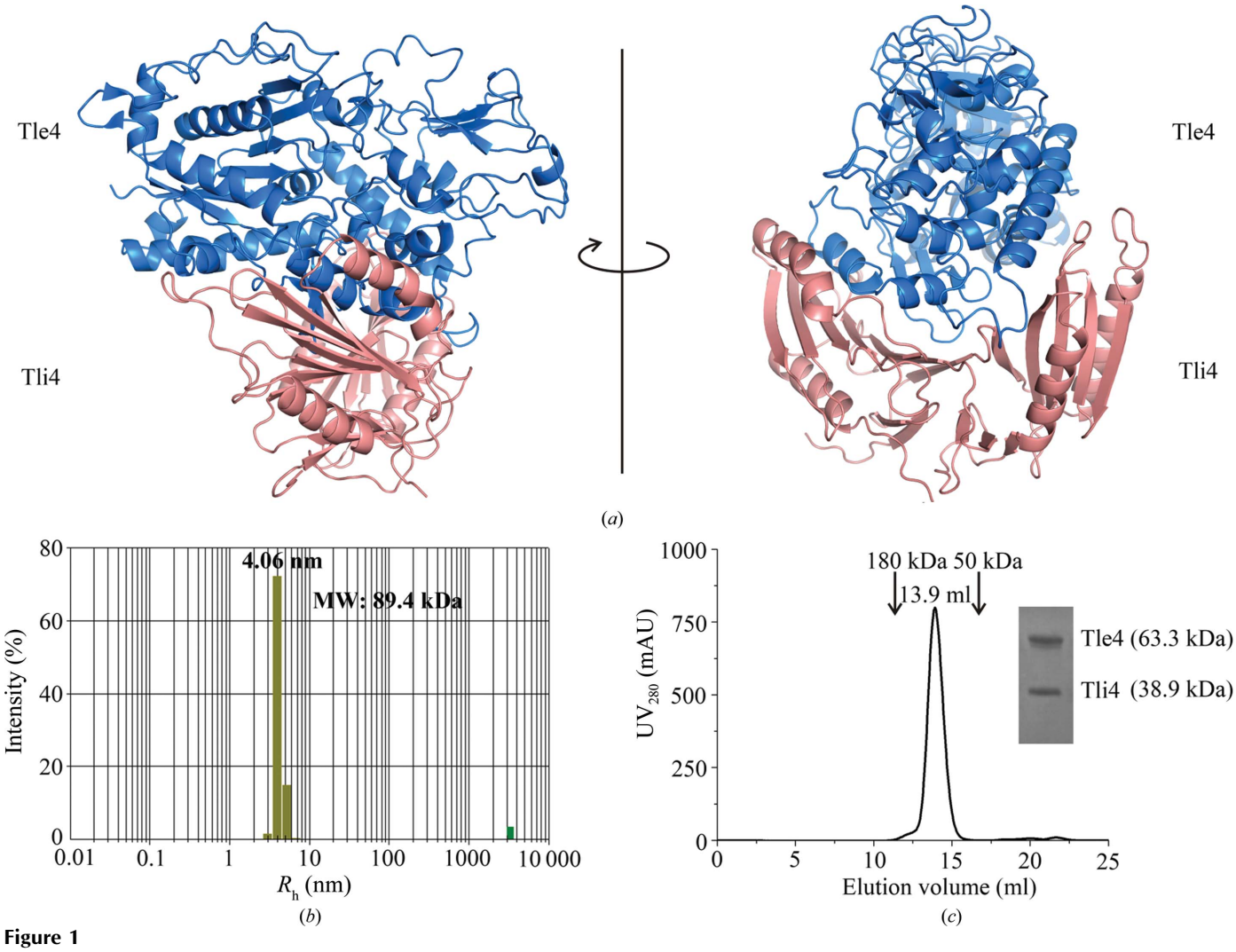

Figure 1
The overall structure of the Tle4–Tli4 complex. (*a*) Cartoon diagram depicting the binary complex, in which Tle4 is shown in marine and Tli4 is shown in salmon. (*b*) Oligomeric state of Tle4–Tli4 determined by dynamic light scattering. The measured average size distributions are consistent with monodisperse particles of average molecular weight ∼89.4 kDa, which is within the expected size range for a Tle4–Tli4 complex with 1:1 binding stoichiomestry. The vertical coordinate axis represents relative dynamic light-scattering intensity and the horizontal coordinate axis represents the hydrodynamic radius (on a logarithmic scale). (*c*) Size-exclusion chromatography of the Tle4–Tli4 complex. The horizontal and vertical axes represent elution volume and ultraviolent absorbance (λ = 280 nm), respectively. The Tle4–Tli4 complex eluted from a Superdex 200 10/300 GL column (GE Healthcare) at approximately 13.9 ml, corresponding to a molecular weight of about 102 kDa. Inset, Coomassie Blue staining of the peak fractions after SDS–PAGE.

is observed in this domain (Fig. 2*b*). As revealed by the electron density ($2F_o - F_c$ and $F_o - F_c$), and the manner in which the ion is coordinated, the coordinating atoms are O atoms that form a pentagonal bipyramid with an average coordinating bond length of approximately 2.51 Å, and we assigned a calcium ion in this site. Furthermore, when the ion at this site was refined as a calcium ion, the *B* factor of this site was similar to those of its coordinating atoms. This calcium ion is coordinated by the bidentate carboxylate of Asp156 and the carboxylate of Glu152 from α4, the carbonyl group of Phe202 and the carboxylate of Asp203 from β7, as well as two water molecules. Because this calcium ion-binding motif is distant from the catalytic centre and the substrate-binding pocket (see the next section), the calcium ion probably plays a role in structural stability rather than a role in the catalytic process. Other bacterial lipases also contain a calcium ion-binding motif (Nardini *et al.*, 2000; Lang *et al.*, 1996; Kim *et al.*, 1997); however, these calcium ion-binding motifs play a role in stabilizing the catalytic histidine residue (Supplementary Fig. S2).

The presence of a conserved α/β-hydrolase fold in Tle4 indicates that the catalytic residues residing in this domain are also invariant. We identified the residues Ser256, His535 and Asp497 as the classical catalytic triad in Tle4 by superposing Tle4 on other structurally related lipases such as *P. cepacia* lipase [PCL; root-mean-square deviation (r.m.s.d.) of 2.7 Å; sequence identity 19%; *DALI Z*-score 15.8], *P. glumae* lipase (PGL; r.m.s.d. of 3.3 Å; sequence identity 21%; *DALI Z*-score 9.5) and *P. aeruginosa* lipase (PAL; r.m.s.d. of 2.7 Å; sequence identity 15%; *DALI Z*-score 15.9), and these three catalytic residues all display a similar permutation in the active site (Fig. 3*a*). The residue Ser256 is the nucleophile located at one

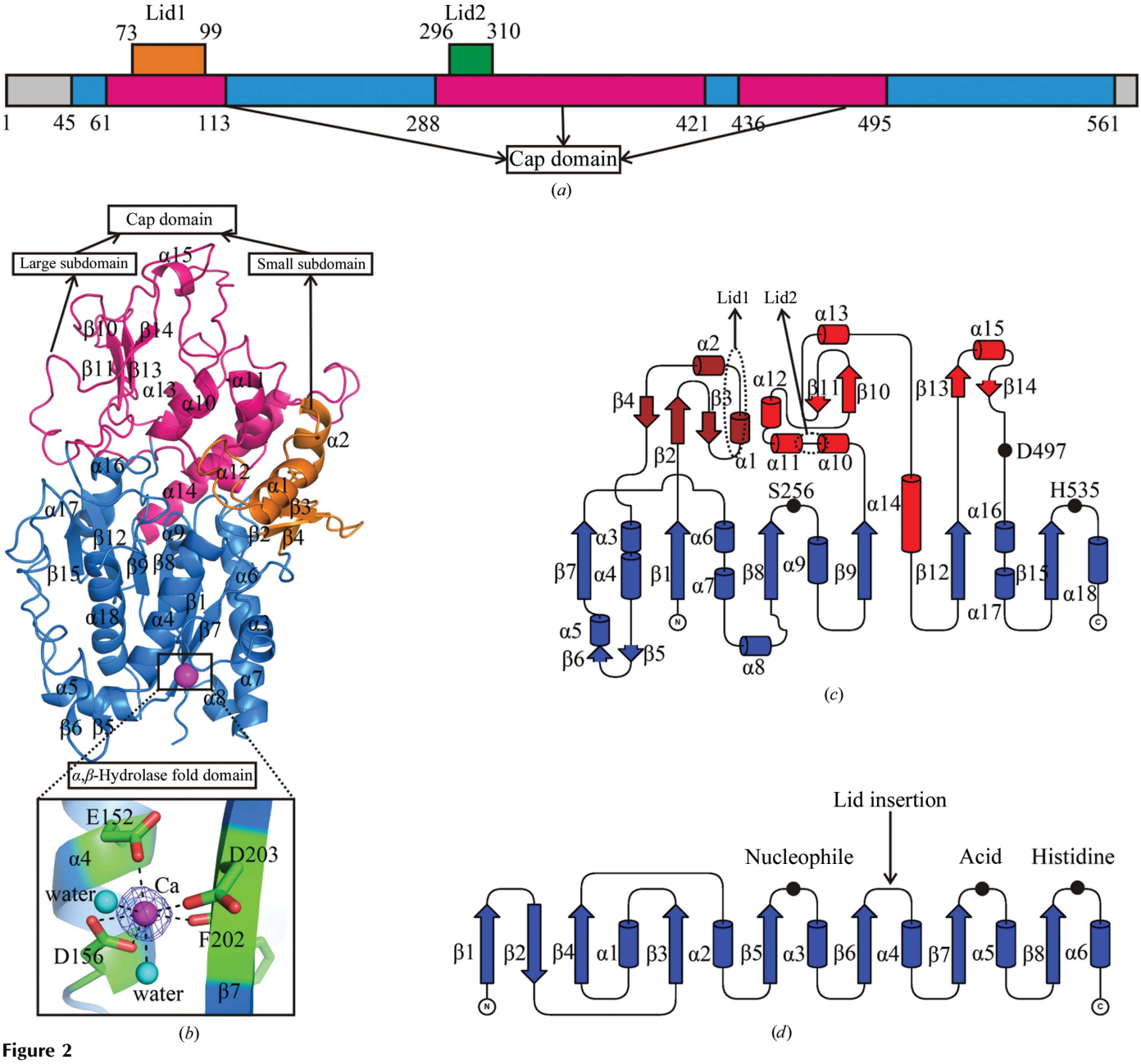

Figure 2
Overall structure of Tle4. (*a*) Schematic representation of Tle4. The grey box denotes the disordered region in the structure, the hot pink box denotes the cap domain, the blue box denotes the α/β-hydrolase fold domain and the lid regions are shown as orange and green boxes. (*b*) The structure of Tle4 is shown as a cartoon. The α/β-hydrolase fold domain is depicted in marine, the large subdomain of the cap domain is depicted in hot pink and the small subdomain of the cap domain is depicted in orange. Secondary-structure elements referred to in the text are labelled. The calcium ion-binding motif is shown, in which the coordinated residues are shown as ball-and-stick models, and water and calcium molecules are shown as spheres in cyan and magenta, respectively. The $2F_o - F_c$ electron-density map for the calcium ion is contoured at 2σ. (*c*, *d*) Topology diagram of Tle4 and the canonical α/β-hydrolase fold. β-Strands are shown as arrows and α-helices are shown as columns. The secondary-structure elements located in the large and small subdomains of the cap domain in Tle4 are depicted in red and brown, respectively, and the canonical α/β-hydrolase fold is depicted in blue. The catalytic triads are marked with black circles. The lid regions in Tle4 are marked by a black dashed ellipse. The lid insertions in homologous proteins to Tle4 are also indicated.

γ-turn between β8 and α9 which is also referred to as the nucleophile elbow (Lenfant *et al.*, 2013). The main chain of the nucleophile adopts unfavourable torsion angles (φ = 57.77°, ψ = −133.54°), as commonly observed in other enzymes containing an α/β-hydrolase fold (Nardini & Dijkstra, 1999; Derewenda & Sharp, 1993). However, instead of the most commonly observed pentapeptide motif G-*X*-S-*X*-G (where *X* denotes any residue) that is commonly present around this nucleophile, Tle4 features a T-*X*-S-*X*-G variation. Because of the steric constraints presented by this sharp turn, Gly, which does not possess a side chain, might be the most favourable choice in the motif (Ollis *et al.*, 1992). In Tle4, the first Gly was replaced by Thr, but the steric problem resulting from the Gly/Thr substitution is solved by a shift of the main chain between

β8 and α9 (Fig. 3*a*). The second triad residue of His535 is situated in a loop connecting β15 and α18; the $N^{\varepsilon 2}$ and $N^{\delta 1}$ atoms of its imidazolium ring form hydrogen bonds to the O^{γ} atom of Ser256 and the $O^{\delta 1}$ atom of Asp497, respectively. As in other members of the α/β-hydrolase fold proteins, the histidine acts as a general base residue to abstract the proton from the catalytic Ser. The resultant positive-charged histidine could then be stabilized by the third triad residue of Asp during catalysis, thus forming the well known charge-relay system (Matthews *et al.*, 1967; Dodson & Wlodawer, 1998).

Another important feature of α/β-hydrolases is the formation of an oxyanion hole together with certain electrophiles during the catalytic process, which plays a key role in stabilizing the tetrahedral intermediate or oxyanion of the substrate. The oxyanion hole is typically created by two peptide NH groups in the vicinity of the nucleophile, and this structural element has been identified in several structurally related lipases, such as PCL (PDB entry 1oil; Kim *et al.*, 1997), PAL (PDB entry 1ex9; Nardini *et al.*, 2000) and PGL (PDB entry 1qge; Noble *et al.*, 1993). By superposition of these structures, we identified the backbone N atoms of the residues Met257 and Ile57 as candidates for forming the oxyanion hole in Tle4 (Fig. 3*b*). In the open-conformation structure of PCL, one water molecule occupies the oxyanion hole and the backbone N atoms of Gln88 and Leu17 form hydrogen bonds to this water molecule (Fig. 3*c*). Similarly, in the ligand-binding open-conformation structure of PAL, the backbone N atoms of His83 and Met16 trapped a tetrahedral intermediate in the oxyanion hole (Fig. 3*d*). In contrast to these two preformed oxyanion holes, the main chain of Leu17 in PGL was moved away from Gln88 and the nucleophile Ser87, resulting in the collapse of the oxyanion hole in the closed-conformation structure (Fig. 3*e*). In the Tle4 structure, these two residues (Met257 and Ile57) are much closer than the equivalent oxyanion-hole residues in PCL and PAL. The side chain of Ile57 fully occupies the position of the water or the tetrahedral intermediate, and thus there is no preformed oxyanion hole in the Tle4–Tli4 complex (Fig. 3*f*).

In addition to this conserved α/β-hydrolase fold domain, Tle4 has evolved a cap domain covering the catalytic triad, as observed in other structurally related lipases. The cap domain in Tle4 can also be divided into two subdomains (the small subdomain and the large subdomain; Figs. 2*b* and 4*a*). The small subdomain consists of two helices (α1 and α2) and one antiparallel sheet (β2,

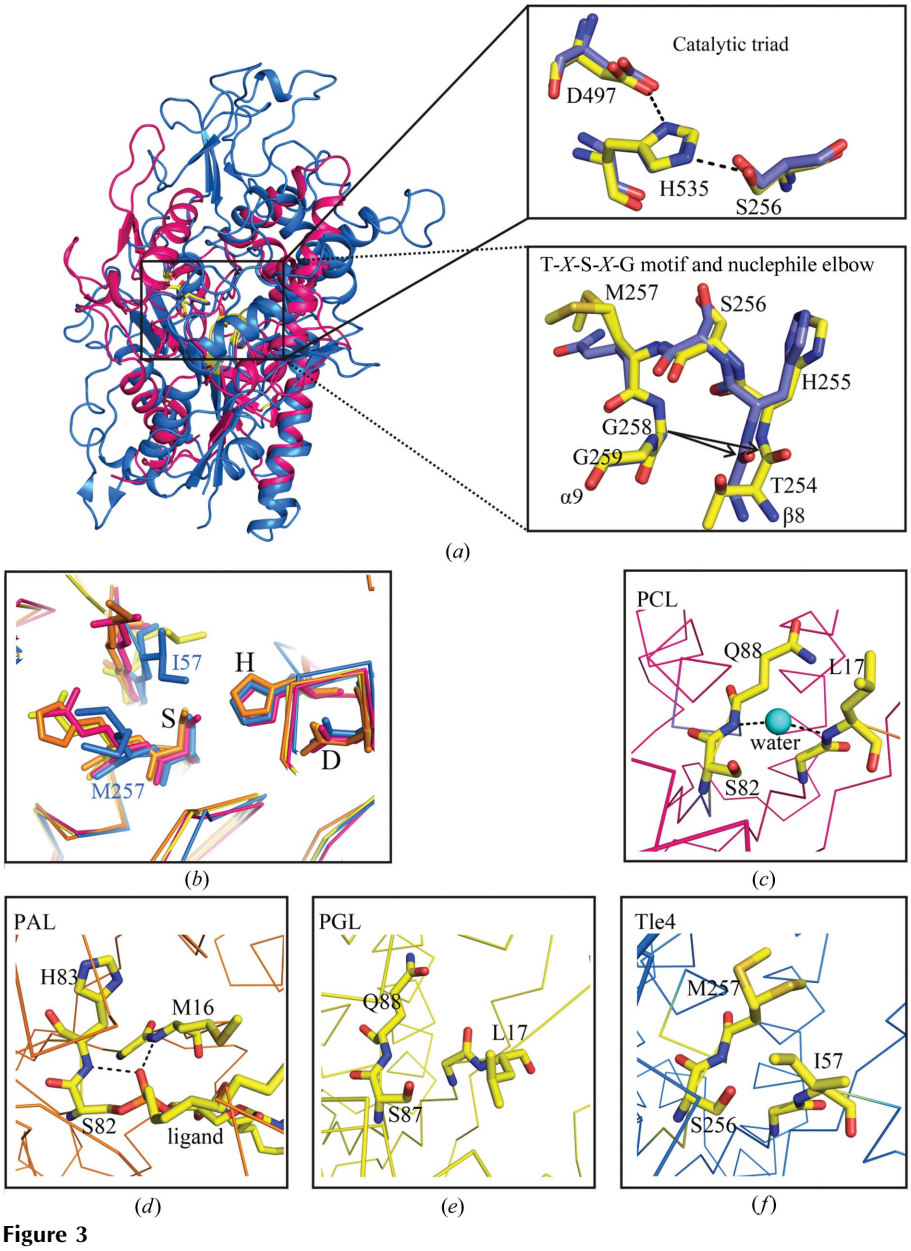

Figure 3
Catalytic centre of Tle4. (*a*) Superposition of Tle4 and the lipase PCL (PDB entry 1oil). Tle4 and PCL are shown as cartoons in marine and hot pink, respectively (left panel). The catalytic triads are shown as ball-and-stick models and hydrogen bonds are labelled as black dashes (in the top right panel). The nucleophile elbows are depicted as sticks, and distances between the main chains are shown as arrows. All labels correspond to Tle4. (*b*) Ribbon alignments between Tle4 and related lipases highlighting the catalytic triads and oxyanion holes. Tle4 is represented in marine, PCL (PDB entry 1oil) in hot pink, PAL (PDB entry 1ex9) in orange and PGL (PDB entry 1qge) in yellow. The residues implicated in catalytic triads and oxyanion holes are depicted as ball-and-stick models. The residues in Tle4 involved in oxyanion-hole formation are labelled in marine. (*c*–*f*) Detailed geometrical comparisons of these lipases (PCL, PAL, PGL and Tle4) involved in the formation of oxyanion holes. The structures are shown as ribbons and the residues are shown as ball-and-stick models. The water molecule is represented as a sphere in cyan. Hydrogen bonds are shown as black dashes.

β3 and β4), and the large subdomain is composed of six helices (α10, α11, α12, α13, α14 and α15) and one β-sheet (β10, β11, β13 and β14). By closely analyzing the Tle4 structure, we identified two lid regions (lid1 and lid2) shielding the catalytic centre. The lid1 region is located in the small subdomain and includes helix α1 and two loops (loop1 between β3 and α1 and loop2 between α1 and α2). Helix α1 mainly consists of hydrophobic residues such as Trp, Leu, Ile, Ala and Phe and is highly hydrophobic; thus, we call it the hydrophobic helix. The loop between α10 and α11 (loop3) in the large subdomain forms the lid2 region, which is located just above the catalytic triad. The hydrophobic residues (Tyr298, Ile301, Ala302, Val304 and Leu306) in loop3 line up against the active site, and loop3 (in lid2) is partially covered by loop1 of the lid1 region, forming a dual-door system that protects the active site from the solvent and holds Tle4 in a closed conformation.

Notably, the cap domain in Tle4 is different from that found in structurally related proteins. The cap domain in Tle4 does not exhibit any sequence or structural similarity to these regions in the other bacterial lipases (PCL, PAL, PGL and CVL). In other bacterial lipases the lids mainly contain one versatile helix, whereas in Tle4 two overlapping loops (the dual-door system) and one hydrophobic helix (α1) serve as the lid regions (lid1 and lid2; Fig. 4); the lids in the other bacterial lipases are located between β6 and α4 (the secondary-structure assignments are in line with the canonical α/β-hydrolase fold; Nardini *et al.*, 2000), but in Tle4 lid1 is located between β3 and α1 and lid2 between β6 and α4 (Figs. 2*c* and 2*d*).

3.3. The structure of Tli4 reveals a crab claw-like conformation

In the structure of the Tle4–Tli4 complex, Tli4 displays a two-domain conformation (domains I and II; Fig. 5*a*) and contains 17 β-strands and four helices (Fig. 5*b* and Supplementary Fig. S3). As shown in Fig. 5(*a*), these two domains pack into a crab claw-like conformation functioning as an inhibitor of Tle4. Both domains adopt an α+β architecture. Domain I features a central antiparallel β-sheet (β4, β5, β6, β7 and β8) sandwiched by two helices (α1 and α2) and a short antiparallel β-sheet (β9, β10 and β11); domain II comprises one β-sheet (β3 and β12–β17) flanked by two α-helices (α3 and α4) and two antiparallel β-strands (β1 and β2). Interestingly, these two domains show a similar topology and fold, although there are two more β-strands in the central β-sheet region in domain II than in domain I (Figs. 5*b*, 6*a* and 6*b*). Superposition of the two domains revealed an r.m.s.d. of approximately 2.7 Å with 83 aligned residues. Further structural comparison using the *DALI* server (Holm & Rosenström, 2010) revealed an unexpected similarity in fold (especially for domain II) between Tli4 and Tsi3, which is the cognate immunity protein of the effector protein Tse3 in *P. aeruginosa* (Russell *et al.*, 2011; Li *et al.*, 2013; Wang *et al.*, 2013; Lu *et al.*, 2014), despite their sequence identity being only about 7% (for 126 residues). On aligning with Tsi3 (PDB entry 4n7s) using *DALI*, the *Z*-score is 9.5 and the calculated r.m.s.d. is approximately 3.4 Å for 126 aligned residues. The only structural difference between them is the presence of a one-helix (α3) insertion between β13 and β14 in Tli4 (Figs. 6*b* and 6*c*). The structural and topological similarities among T6SS effector immunity proteins might provide clues regarding their evolutionary relationships.

3.4. Complex structure and inhibitory mechanism

The interactions between Tle4 and Tli4 are considerably extensive (Supplementary Table S1). Interface analysis by

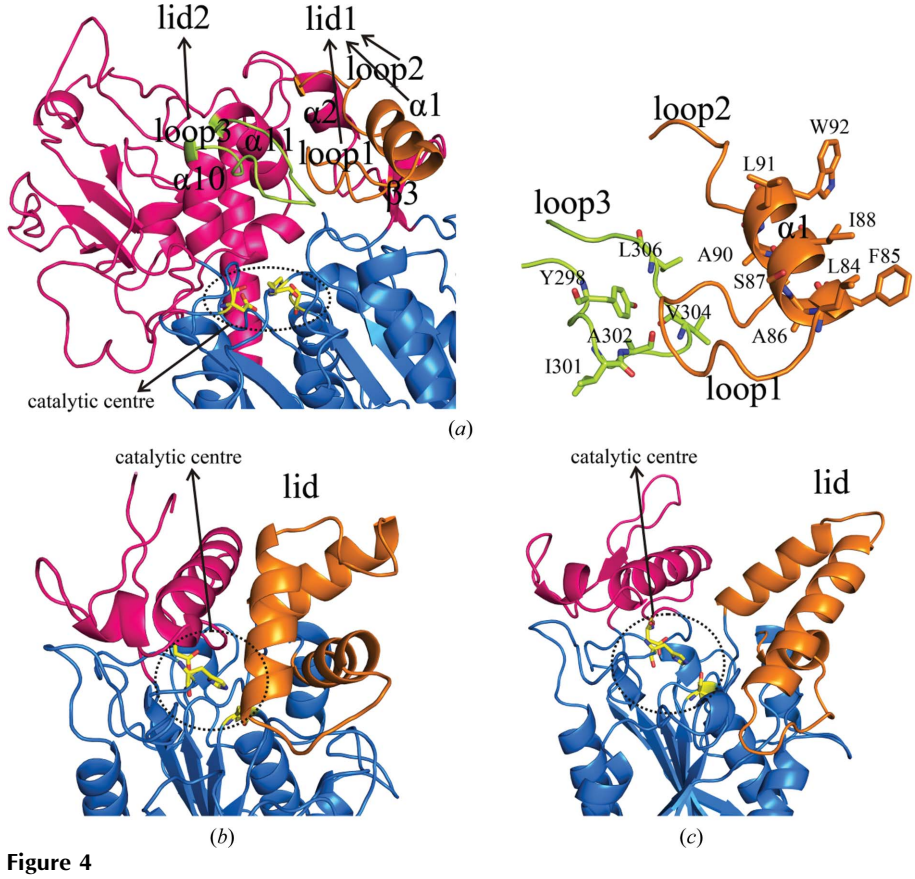

Figure 4
Cap domain of Tle4 in a closed conformation. (*a*) Tle4 is shown as a cartoon. In the left panel the α/β-hydrolase fold domain is shown in blue, the cap domain is shown in hot pink and lid1 and lid2 in the cap domain are depicted in orange and yellow, respectively. The right panel shows detail of the lid1 and lid2 region, and the residues in these regions are depicted as sticks. The catalytic triad is also shown as sticks. (*b*, *c*) The cap domains of the lipases PGL (PDB entry 1qge) and PCL (PDB entry 1oil) in closed and open conformations, respectively. α/β-Hydrolase fold domains are shown in blue and cap domains are shown in hot pink. The lid regions in the cap domain are shown in orange. The catalytic triads are represented as sticks.

PISA (Krissinel & Henrick, 2007) shows that the interaction area is about 2854.9 Å^2, which covers roughly 13.3% of the solvent-accessible surface area of Tle4 (21 441.8 Å^2) and 18.7% of the solvent-accessible surface area of Tli4 (15 286.0 Å^2). Tli4 uses its two domains to interact with the cap domain of Tle4, with domain II of Tli4 binding to the small subdomain and domain I binding to large subdomain of Tle4 (Fig. 7). In the former binding interface the interaction around the lid1 region of Tle4 is extensive: helix α1 in lid1 is trapped by a hydrophobic pocket in domain II of Tli4. The latter interaction interface is mainly mediated through loops and the interaction area is smaller than that of the former. Thus, the interaction in the latter part might play an auxiliary role in complex formation. The curtaining of the Tle4 cap domain, especially the grasping of the Tle4 lid1 by Tli4, should definitely prevent interfacial activation of Tle4. Therefore, in the self-protection process, Tle4, which is captured in a closed conformation in the complex, is catalytically disabled by Tli4.

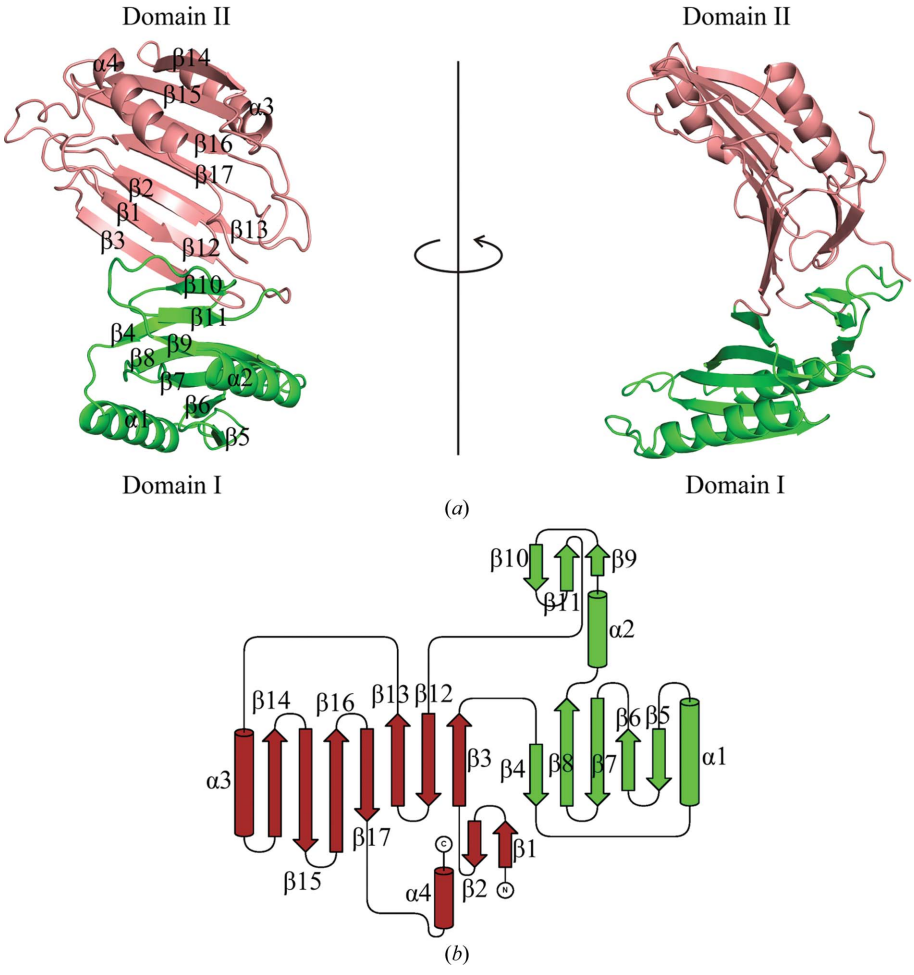

Figure 5
Overall structure of Tli4. (*a*) The structure of Tli4 is represented as a cartoon. Domain I is coloured green and domain II is coloured salmon. The secondary-structure elements referred to in the text are labelled. (*b*) Topology diagram of Tli4. β-Strands are shown as arrows and α-helices are shown as columns. The secondary-structure elements located in domains I and II of Tli4 are depicted in green and brown, respectively.

4. Discussion

Tle4 (PA1510) is a putative effector that is transported to the periplasm of the neighbouring cells by H2-T6SS in *P. aeruginosa* and functions as a phospholipase that degrades the cell membrane. The structure of Tle4 displays a lipase-like fold with two domains, as observed in other lipases. One domain is the canonical α/β-hydrolase fold domain, in which the conserved catalytic triad (Ser256,

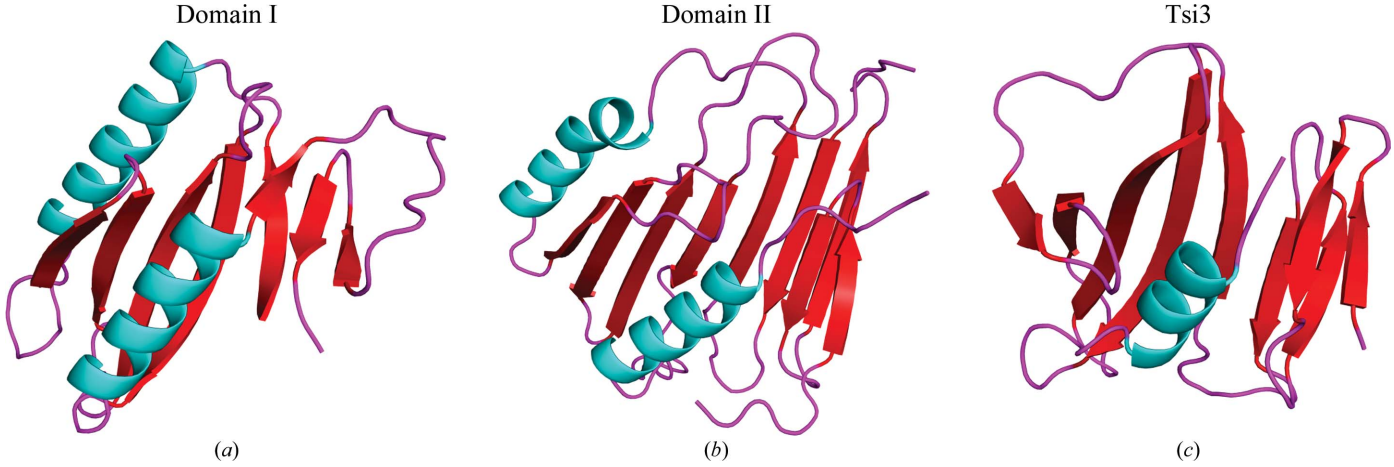

Figure 6
Structural comparisons among domain I and domain II of Tli4 and Tsi3 (PDB entry 4n7s). Loops, α-helices and β-strands are coloured purple, cyan and red, respectively. (*a*) Cartoon representation of domain I of Tli4. (*b*) Cartoon representation of domain II of Tli4. (*c*) Cartoon representation of Tsi3.

His535 and Asp497) was identified. The residue Ser256 is located at the featured nucleophile elbow but within an unusual pentapeptide motif (T-*X*-S-*X*-G), which differs from other canonical α/β-hydrolases with the G-*X*-S-*X*-G motif. The steric hindrance in the sharp turn is relieved by a main-chain shift, which has also been described as an 'opening' of the nucleophile elbow as observed in *V. harveyi* thioesterase (Lawson *et al.*, 1994). In the oxyanion hole, the close distance between Met257 and Ile57 in Tle4 indicates a collapsed oxyanion architecture, the reversion of which possibly requires a movement of lid1 that would cause a shift between Met257 and Ile57. Except for small variations in the secondary-structure elements (*e.g.* a β-sheet insertion in the surrounding helices and the presence of a calcium-binding motif), this domain in Tle4 exhibits the characteristics of a canonical α/β-hydrolase fold. The other domain in Tle4 is the cap domain, which is also widely observed in lipases. However, the cap domain in Tle4 shows unique features that differ completely from those of other lipases such as PAL, PGL, PCL and CVL. Instead of containing only a few helices that cover the catalytic site, the cap domain in Tle4 is larger and more complex in structural composition. More interestingly, Tle4 possesses two lid regions, with one stacking on the other, thereby forming a dual-door system that buries the catalytic triad in a deep funnel. The presence of an unusual cap domain indicates that Tle4 might be activated by a mechanism that is distinct from the regulatory mechanism observed in other bacterial lipases. We suggest that when Tle4 is transported to the recipient cells, the encounter with the membrane might enable its highly hydrophobic helix $\alpha1$ to bind and probably become buried in the hydrophobic core of the phospholipid bilayer, subsequently enabling the opening of the dual-door

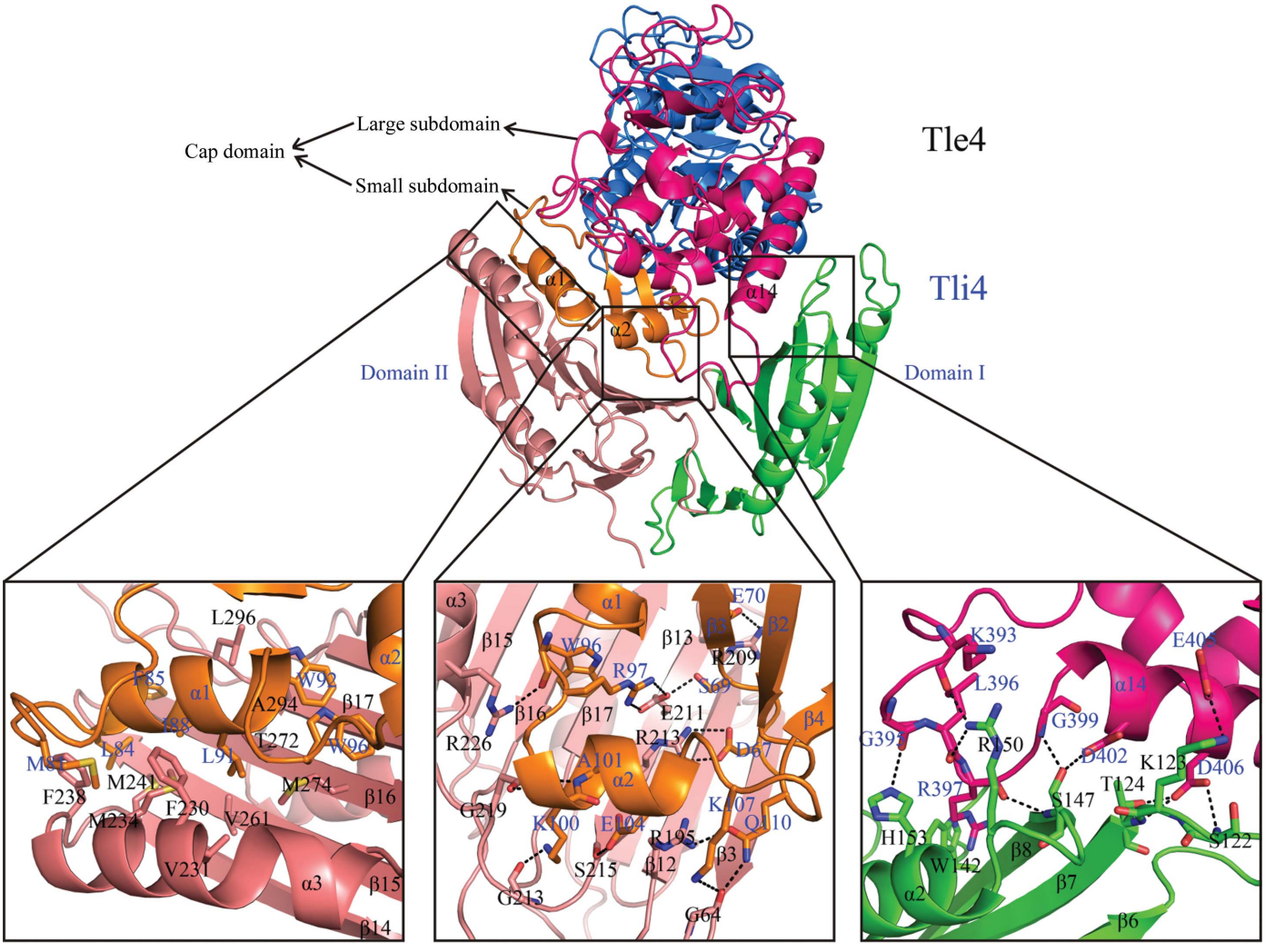

Figure 7
Detailed interactions between Tle4 and Tli4. The top panel shows the complex of Tle4 and Tli4 represented as a cartoon. The α/β-hydrolase fold domain of Tle4 is coloured blue, the small subdomain of the cap domain is shown in orange and the large subdomain of cap domain is shown in hot pink. Domain I and domain II in Tli4 are shown as green and salmon cartoons, respectively. The bottom panel on the left shows the hydrophobic interaction between the small subdomain of Tle4 and domain II of Tli4, the bottom panel in the centre displays the hydrogen bonds and salt-bridge network between the small subdomain of Tle4 and domain II of Tli4 and the bottom panel on the right highlights the interface between the large subdomain of Tle4 and domain I of Tli4. The residues from Tle4 and Tli4 are illustrated as ball-and-stick models. The black dashed lines represent hydrogen bonds and salt bridges.

system expose the active site to the phospholipid. Simultaneously, the movement of the lid region would result in the formation of the oxyanion hole in the active site and finally lead to the activation of Tle4. Thus, Tle4 probably obeys an interfacial activation mechanism that involves the structural rearrangement observed in neutral lipases (Brzozowski *et al.*, 1991; Derewenda *et al.*, 1992). This type of interfacial activation differs from the mechanism used by some other phospholipases, such as the low-molecular-weight PLA_2s secreted by reptiles (Scott *et al.*, 1990). As a proposed phospholipase, we attempted to identify the substrate selectivity of Tle4 on the *sn*-1 and *sn*-2 moieties in phospholipids. However, Tle4 is highly insoluble when overexpressed in *E. coli* even in the presence of a fusion tag such as MBP or GST, which made it impossible to perform related biochemical experiments. Therefore, other methods need to be explored to examine its selectivity.

Tli4, the cognate immunity protein of Tle4, possesses two domains (domain I and domain II), both of which display a similar fold and topology. A homologous fold was also discovered in another T6SS immunity protein, Tsi3. This raises the question whether this fold is widespread in T6SS immunity proteins, and further studies on the structures of these proteins are required to address this question. Moreover, Tli4 uses a β-sheet in the domain II for function, whereas Tsi3 employs three loops for this purpose.

In the Tli4–Tle4 complex structure, Tli4 uses its two domains to interact with the cap domain of Tle4 and thereby prevents the interfacial activation of Tle4. This bipartite interaction mode is very distinctive among those described in T6SS E–I pairs. To date, the structures of several E–I pair complexes have been solved, and the main inhibitory mechanism used in those pairs involves the insertion of the immunity protein into the substrate-binding pocket of the effector protein, which prevents the effector protein binding to its substrate (Ding *et al.*, 2012; Benz *et al.*, 2012, 2013; Shang *et al.*, 2012; English *et al.*, 2012; Zhang *et al.*, 2013, 2014; Dong, Zhang *et al.*, 2013; Li *et al.*, 2013; Wang *et al.*, 2013; Whitney *et al.*, 2013; Yang *et al.*, 2014; Lu *et al.*, 2014). In contrast to this insertion-inactivation mechanism, Tli4 inhibits Tle4 using a grasp-inactivation mechanism. The variant inhibitory strategies indicate a diversified E–I pair interaction mode in T6SS.

As discussed above, our structural analysis of the Tle4–Tli4 complex reveals the molecular mechanism underlying the self-protection of *P. aeruginosa* and expands our understanding of the role of T6SS in bacterial competition.

We would like to thank the staff of beamline BL17U1 at Shanghai Synchrotron Radiation Facility (SSRF) for support with data collection and Dr Lu Guangwen for his critical reading of the manuscript. This work was financially supported by the National Natural Science Foundation of China (Grant Nos. 31400634 and 31201008), the Key Clinical Specialty Discipline Construction Program of Fujian, People's Republic of China, the Key Project of National Science and Technology of China (Grant Nos. 2012ZX10002010-001-006 and 2012ZX10002016-013), the Scientific Foundation of Fuzhou Health Department (Grant Nos. 2013-S-wq16 and 2013-S-wp1) and the Research Development Foundation of Fujian Medical University (Grant Nos. FZS13001Y and FZS13005Z).

References

Adams, P. D., Grosse-Kunstleve, R. W., Hung, L.-W., Ioerger, T. R., McCoy, A. J., Moriarty, N. W., Read, R. J., Sacchettini, J. C., Sauter, N. K. & Terwilliger, T. C. (2002). *Acta Cryst.* D**58**, 1948–1954.
Benz, J. & Meinhart, A. (2014). *Curr. Opin. Microbiol.* **17**, 1–10.
Benz, J., Reinstein, J. & Meinhart, A. (2013). *PLoS One*, **8**, e67362.
Benz, J., Sendlmeier, C., Barends, T. R. & Meinhart, A. (2012). *PLoS One*, **7**, e40453.
Bingle, L. E., Bailey, C. M. & Pallen, M. J. (2008). *Curr. Opin. Microbiol.* **11**, 3–8.
Brooks, T. M., Unterweger, D., Bachmann, V., Kostiuk, B. & Pukatzki, S. (2013). *J. Biol. Chem.* **288**, 7618–7625.
Brunet, Y. R., Hénin, J., Celia, H. & Cascales, E. (2014). *EMBO Rep.* **15**, 315–321.
Brzozowski, A. M., Derewenda, U., Derewenda, Z. S., Dodson, G. G., Lawson, D. M., Turkenburg, J. P., Bjorkling, F., Huge-Jensen, B., Patkar, S. A. & Thim, L. (1991). *Nature (London)*, **351**, 491–494.
Cascales, E. & Cambillau, C. (2012). *Philos. Trans. R. Soc. Lond. B Biol. Sci.* **367**, 1102–1111.
Coulthurst, S. J. (2013). *Res. Microbiol.* **164**, 640–654.
Derewenda, Z. S., Derewenda, U. & Dodson, G. G. (1992). *J. Mol. Biol.* **227**, 818–839.
Derewenda, Z. S. & Sharp, A. M. (1993). *Trends Biochem. Sci.* **18**, 20–25.
Ding, J., Wang, W., Feng, H., Zhang, Y. & Wang, D.-C. (2012). *J. Biol. Chem.* **287**, 26911–26920.
Dodson, G. & Wlodawer, A. (1998). *Trends Biochem. Sci.* **23**, 347–352.
Dong, T. G., Ho, B. T., Yoder-Himes, D. R. & Mekalanos, J. J. (2013). *Proc. Natl Acad. Sci. USA*, **110**, 2623–2628.
Dong, C., Zhang, H., Gao, Z.-Q., Wang, W.-J., She, Z., Liu, G.-F., Shen, Y.-Q., Su, X.-D. & Dong, Y.-H. (2013). *Biochem. J.* **454**, 59–68.
Durand, E., Cambillau, C., Cascales, E. & Journet, L. (2014). *Trends Microbiol.* **22**, 498–507.
Emsley, P. & Cowtan, K. (2004). *Acta Cryst.* D**60**, 2126–2132.
English, G., Trunk, K., Rao, V. A., Srikannathasan, V., Hunter, W. N. & Coulthurst, S. J. (2012). *Mol. Microbiol.* **86**, 921–936.
Filloux, A. (2013). *F1000Prime Rep.* **5**, 52.
Hachani, A., Allsopp, L. P., Oduko, Y. & Filloux, A. (2014). *J. Biol. Chem.* **289**, 17872–17884.
Ho, B. T., Dong, T. G. & Mekalanos, J. J. (2014). *Cell Host Microbe*, **15**, 9–21.
Holm, L. & Rosenström, P. (2010). *Nucleic Acids Res.* **38**, W545–W549.
Hood, R. D. *et al.* (2010). *Cell Host Microbe*, **7**, 25–37.
Jiang, F., Waterfield, N. R., Yang, J., Yang, G. & Jin, Q. (2014). *Cell Host Microbe*, **15**, 600–610.
Kabsch, W. (1976). *Acta Cryst.* A**32**, 922–923.
Kapitein, N. & Mogk, A. (2013). *Curr. Opin. Microbiol.* **16**, 52–58.
Kim, K. K., Song, H. K., Shin, D. H., Hwang, K. Y. & Suh, S. W. (1997). *Structure*, **5**, 173–185.
Koskiniemi, S., Lamoureux, J. G., Nikolakakis, K. C., t'Kint de Roodenbeke, C., Kaplan, M. D., Low, D. A. & Hayes, C. S. (2013). *Proc. Natl Acad. Sci. USA*, **110**, 7032–7037.
Krissinel, E. & Henrick, K. (2007). *J. Mol. Biol.* **372**, 774–797.
Lang, D., Hofmann, B., Haalck, L., Hecht, H.-J., Spener, F., Schmid, R. D. & Schomburg, D. (1996). *J. Mol. Biol.* **259**, 704–717.
Lawson, D. M., Derewenda, U., Serre, L., Ferri, S., Szittner, R., Wei, Y., Meighen, E. A. & Derewenda, Z. S. (1994). *Biochemistry*, **33**, 9382–9388.

Leiman, P. G., Basler, M., Ramagopal, U. A., Bonanno, J. B., Sauder, J. M., Pukatzki, S., Burley, S. K., Almo, S. C. & Mekalanos, J. J. (2009). *Proc. Natl Acad. Sci. USA*, **106**, 4154–4159.
Lenfant, N., Hotelier, T., Velluet, E., Bourne, Y., Marchot, P. & Chatonnet, A. (2013). *Nucleic Acids Res.* **41**, D423–D429.
Li, L., Zhang, W., Liu, Q., Gao, Y., Gao, Y., Wang, Y., Wang, D. Z., Li, Z. & Wang, T. (2013). *J. Biol. Chem.* **288**, 30607–30613.
Lu, D. *et al.* (2014). *Mol. Microbiol.* **92**, 1092–1112.
Ma, L.-S., Hachani, A., Lin, J.-S., Filloux, A. & Lai, E.-M. (2014). *Cell Host Microbe*, **16**, 94–104.
Matthews, B. W., Sigler, P. B., Henderson, R. & Blow, D. M. (1967). *Nature (London)*, **214**, 652–656.
Miyata, S. T., Unterweger, D., Rudko, S. P. & Pukatzki, S. (2013). *PLoS Pathog.* **9**, e1003752.
Nardini, M. & Dijkstra, B. W. (1999). *Curr. Opin. Struct. Biol.* **9**, 732–737.
Nardini, M., Lang, D. A., Liebeton, K., Jaeger, K. E. & Dijkstra, B. W. (2000). *J. Biol. Chem.* **275**, 31219–31225.
Noble, M. E., Cleasby, A., Johnson, L. N., Egmond, M. R. & Frenken, L. G. (1993). *FEBS Lett.* **331**, 123–128.
Ollis, D. L., Cheah, E., Cygler, M., Dijkstra, B., Frolow, F., Franken, S. M., Harel, M., Remington, S. J., Silman, I., Schrag, J., Sussman, J. L., Verschueren, K. H. G. & Goldman, A. (1992). *Protein Eng.* **5**, 197–211.
Otwinowski, Z. & Minor, W. (1997). *Methods Enzymol.* **276**, 307–326.
Pell, L. G., Kanelis, V., Donaldson, L. W., Howell, P. L. & Davidson, A. R. (2009). *Proc. Natl Acad. Sci. USA*, **106**, 4160–4165.
Pukatzki, S., Ma, A. T., Revel, A. T., Sturtevant, D. & Mekalanos, J. J. (2007). *Proc. Natl Acad. Sci. USA*, **104**, 15508–15513.
Russell, A. B., Hood, R. D., Bui, N. K., LeRoux, M., Vollmer, W. & Mougous, J. D. (2011). *Nature (London)*, **475**, 343–347.
Russell, A. B., LeRoux, M., Hathazi, K., Agnello, D. M., Ishikawa, T., Wiggins, P. A., Wai, S. N. & Mougous, J. D. (2013). *Nature (London)*, **496**, 508–512.
Russell, A. B., Peterson, S. B. & Mougous, J. D. (2014). *Nature Rev. Microbiol.* **12**, 137–148.
Russell, A. B., Singh, P., Brittnacher, M., Bui, N. K., Hood, R. D., Carl, M. A., Agnello, D. M., Schwarz, S., Goodlett, D. R., Vollmer, W. & Mougous, J. D. (2012). *Cell Host Microbe*, **11**, 538–549.
Schwarz, S., Singh, P., Robertson, J. D., LeRoux, M., Skerrett, S. J., Goodlett, D. R., West, T. E. & Mougous, J. D. (2014). *Infect. Immun.* **82**, 1445–1452.
Scott, D. L., White, S. P., Otwinowski, Z., Yuan, W., Gelb, M. H. & Sigler, P. B. (1990). *Science*, **250**, 1541–1546.
Shang, G., Liu, X., Lu, D., Zhang, J., Li, N., Zhu, C., Liu, S., Yu, Q., Zhao, Y., Zhang, H., Hu, J., Cang, H., Xu, S. & Gu, L. (2012). *Biochem. J.* **448**, 201–211.
Silverman, J. M., Brunet, Y. R., Cascales, E. & Mougous, J. D. (2012). *Annu. Rev. Microbiol.* **66**, 453–472.
Suarez, G., Sierra, J. C., Erova, T. E., Sha, J., Horneman, A. J. & Chopra, A. K. (2010). *J. Bacteriol.* **192**, 155–168.
Terwilliger, T. C. (2000). *Acta Cryst.* D**56**, 965–972.
Terwilliger, T. C. & Berendzen, J. (1999). *Acta Cryst.* D**55**, 849–861.
Toesca, I. J., French, C. T. & Miller, J. F. (2014). *Infect. Immun.* **82**, 1436–1444.
Van Duyne, G. D., Standaert, R. F., Karplus, P. A., Schreiber, S. L. & Clardy, J. (1993). *J. Mol. Biol.* **229**, 105–124.
Wang, T., Ding, J., Zhang, Y., Wang, D.-C. & Liu, W. (2013). *Acta Cryst.* D**69**, 1889–1900.
Whitney, J. C., Beck, C. M., Goo, Y. A., Russell, A. B., Harding, B. N., De Leon, J. A., Cunningham, D. A., Tran, B. Q., Low, D. A., Goodlett, D. R., Hayes, C. S. & Mougous, J. D. (2014). *Mol. Microbiol.* **92**, 529–542.
Whitney, J. C., Chou, S., Russell, A. B., Biboy, J., Gardiner, T. E., Ferrin, M. A., Brittnacher, M., Vollmer, W. & Mougous, J. D. (2013). *J. Biol. Chem.* **288**, 26616–26624.
Yang, X., Xu, M., Wang, Y., Xia, P., Wang, S., Ye, B., Tong, L., Jiang, T. & Fan, Z. (2014). *Acta Cryst.* D**70**, 1094–1103.
Zhang, H., Zhang, H., Gao, Z.-Q., Wang, W.-J., Liu, G.-F., Xu, J.-H., Su, X.-D. & Dong, Y.-H. (2013). *J. Biol. Chem.* **288**, 5928–5939.
Zhang, J., Zhang, H., Gao, Z., Hu, H., Dong, C. & Dong, Y.-H. (2014). *FEBS Lett.* **588**, 1891–1898.